Faraday tilting of water-immersed granular beds

R. J. Milburn, M. A. Naylor, A. J. Smith, M. C. Leaper, K. Good, Michael R. Swift, and P. J. King
School of Physics and Astronomy, University of Nottingham, Nottingham NG7 2RD, United Kingdom
(Received 2 April 2004; revised manuscript received 17 November 2004; published 28 January 2005)

Under low-frequency vertical vibration, a system of fine grains within a fluid is observed to tilt or to form piles, an effect studied by Faraday for grains in air. Here, we investigate the physical mechanisms behind Faraday tilting in a bed of vertically vibrated bronze spheres fully immersed in water. Experimental observations of surface tilting and bulk convection are compared with the results of molecular dynamics simulations in which the water is treated as an incompressible fluid. Our simulations reproduce the main features observed experimentally. Most tilt construction is shown to be due to horizontal fluid flow within the bed, principally occurring when the gap between the bed and the supporting platform is close to a maximum. Tilt destruction occurs by granular surface flow and in the bulk of the bed at times during each vibratory cycle close to and just later than bed impact. Destruction becomes more important for higher values of frequency and vibration amplitude, leading to lower tilt angles, partial tilting, or the symmetric domed geometry of Muchowski flow.

DOI: 10.1103/PhysRevE.71.011308 PACS number(s): 45.70.−n, 81.05.Rm

I. INTRODUCTION

Since the time of Chladni and Faraday it has been known that fine particulates may spontaneously form conical or domed piles when placed upon a horizontal surface which is being vibrated vertically either by tapping or by continuous oscillation [1]. Grains are seen to "avalanche" down the pile surfaces, the shape being maintained by replenishment from the bulk. Within a vertically vibrated container, a body of grains may be observed to tilt through the same "Faraday effect." Once the tilt has developed, grains "avalanche" down the upper slope, the shape being maintained by asymmetric convective flow within the bulk of the grains [2–4].

Faraday provided evidence that piling is associated with air movement induced by the motion of the vibrated surface and the throwing of the granular bed [1]. The wall friction experienced by grains held within a container may influence the degree of tilt but wall friction alone is not sufficient to cause the tilting observed [5,6]. While the presence of a horizontal component of vibration may have led to reports of tilting in the absence of air [3,7], the evidence that, in a well aligned system, both Faraday piling and tilting result from the involvement of air is now widely accepted [4,5,8–13]. However, the detailed mechanism and some important aspects of the behavior are still the subject of active debate [5,8–13].

When a bed of grains is thrown from its supporting surface by vibration of sufficient amplitude, the air pressure under and within the bed deviates from ambient. Faraday suggested that grains are sucked under the base of the bed early in flight by the lowered air pressure there. Later the bed falls upon these grains, leading to the development of tilt [1]. However, Kumar *et al.* [9], and later Behringer *et al.* [13], have shown that, for modest amplitudes of vibration, only regions of the bed close to the upper surface are involved in maintaining tilting. Further explanations for tilting have been offered. Later in flight, as the bed falls towards the vibrating surface, the pressure below the bed exceeds ambient. Pak *et al.* [5], referring to the work of Gutman [14] and Laroche *et al.* [4], have proposed that it is the upward gas flow resulting from this enhanced pressure, together with the earlier closure of the gap at regions of shallower bed depth, which leads to Faraday tilting. Duran has offered this upward air flow as the explanation for the behavior of very fine beds when tapped in the presence of air [11,12]. Laroche *et al.* [4], noting that not all regions of a tilted thrown bed land at the same time [2], have suggested that it is the internal shearing resulting from the compaction fronts formed at landing which are responsible for tilting. However, Thomas and Squires observed horizontal granular motion earlier in the vibration cycle than the observation of a compaction front. They suggested that it is the horizontal component of the air flow within the bed during flight which leads to Faraday tilting, the motion occurring primarily during the period of reduced pressure under the bed [8,10].

Despite the substantial body of previous work, many aspects of the Faraday tilting effect are not fully understood. In particular, it is important to clarify the principal mechanism for bed tilt, to identify when during the vibration cycle the granular motion which leads to bed tilt occurs and to determine how this granular motion depends upon the amplitude and frequency of vibration. The related issues of why Faraday tilting weakens and vanishes at higher values of frequency also needs to be addressed, as does the involvement of the granular motion at the upper surface.

The study of the granular dynamics of these coupled fluid-grain systems presents challenges both in experiments and in simulation. Following the motion of vibrated fine grains during experiments presents a number of difficulties for high-speed photography. The ability to resolve an individual grain may conflict with observing gross movement. Usually only the surfaces of a granular bed are available for observation and the motion there may not be typical of the bulk. Simulation offers the possibility of probing many properties not easily accessible to experimental investigation. However, simulation too presents a number of challenges, including the difficulty of adequately treating the interactions between the fluid and the grains. At the upper surface of a vibrated bed, the porosity changes rapidly with height. In simulations this variation of porosity must be adequately de-

scribed, since the dynamics at the upper surface affect the granular motion within the bed. The successful simulation of Faraday tilting would be an important step towards understanding a number of fluid effects including binary granular systems where Faraday tilting is involved in many of the separation phenomena which have been observed at low frequencies [15,16].

It has been briefly noted that Faraday tilting may be observed in liquid-immersed granular systems [4]. Here we report a detailed investigation of this effect in a system of fully water-immersed bronze spheres, using both experimentation and computer simulation. Our simulations reproduce very many aspects of the experimental observations and offer penetrating physical insight into the tilting mechanisms. We identify the causes and timings of both tilt construction and destruction and explain why the tilting weakens at higher frequencies and greater amplitudes of vibration. Finally, we discuss the relevance of this work to understanding air-driven Faraday tilting.

II. EXPERIMENTAL TECHNIQUES

The use of a liquid such as water offers a number of advantages for investigating the mechanisms of Faraday tilting. First, water enables considerably larger particles to be used, making the observation of both the fluid and granular dynamics appreciably simpler than for air. For nonturbulent fluid flow, the effects of fluid drag on the granular dynamics are governed by the combination $\rho_g d^2/\eta$, where ρ_g is the density of the granular material, d is the grain diameter, and η is the dynamic viscosity of the surrounding fluid [16]. At 20 °C, water is about 50 times more viscous than air, suggesting that Faraday tilting effects may be observed in water for particles ~ 7 times larger in diameter than for the observation of similar effects in air. The larger grain dimensions greatly aid both the observation of the movement of individual grains and the direct observation of the associated fluid flow through the use of small mica fragments which, when added to the water, closely follow the flow [17].

Second, at low frequencies, spherical particles immersed in water within a smooth walled rectangular box with a horizontal aspect ratio far from unity, provide a system for which the mean granular and fluid behaviours are close to two dimensional. This enables comparison with simulations which assume two-dimensional fluid flow, as is discussed in more detail below.

Finally, the use of water eliminates the effects of static electricity which often slow and otherwise modify the dynamics of dry granular systems when they are shaken vigorously for long periods, particularly within an insulating box.

In our experiments, the granular bed is contained within a rectangular box with smooth soda-glass walls. The box is vibrated sinusoidally and in a direction within ±0.2° of vertical in a manner which ensures accurate one dimensional motion [15,16]. The principal measurements have been carried out using a box of inner dimensions 10×40 mm in the horizontal plane and 50 mm in height. In reporting our observations we refer to the larger 40×50-mm surfaces as the "front" and "back" faces of the box. These two surfaces are described collectively as the "principal faces." The 10×50 -mm surfaces are described as the "side walls." The "mid-plane" of the box is the central plane midway between, and parallel to, the the side walls.

The motion of the box is monitored using cantilever capacitance accelerometer systems which display the dimensionless maximum acceleration $\Gamma = a\omega^2/g$. Here a is the amplitude of vertical vibration, $\omega = 2\pi f$ is the angular frequency, and g is the acceleration due to gravity. The majority of the experiments have been performed using spherical bronze grains of density 8900 kg m^{-3} with a ±10% spread of grain diameters to avoid gross crystallization effects. The grains are inserted through an upper hole and the box is then filled with distilled water. The box is shaken to release any air bubbles and then refilled and sealed so that no visible air bubbles are contained within its volume.

The observation of granular motion or that of the flow tracers is carried out visually and using a high-speed digital camera, operated usually at 1000 frames per second. Software is used to identify the position of each visible grain through light reflected from its surface. The grains are tracked between frames, enabling determination of both the motion of individual particles and the mean convection field. A principal function of the particle tracing software is to distinguish the motion of the particles with respect to the box, from the substantial motion of the box during each vibration cycle.

The convective motion within the bed has also been studied by observing the uniformity of movement at the upper granular surface during vibration, by studying the position of marked grains during convection and by locating their position after vibration is halted.

III. OBSERVATION OF FARADAY TILTING UNDER WATER

We have studied immersed Faraday tilting for ranges of grain size, frequency, Γ, and bed depths. Figure 1 shows, schematically, the equilibrium behavior as a function of f and Γ of a bed of spherical bronze grains with diameters in the range 600–710 μm. The mean vertical depth of the bed is 10 mm. The lower line α is an indication of the onset of appreciable granular convection on the time scale of one minute. Convection below this line may be observed, but on progressively longer time scales as Γ is reduced.

At higher frequencies, in the region shown as A, the convection is of Muchowski form [18], consisting of a pair of symmetric convection rolls with upward granular motion close to the mid-plane of the box and downwards motion principally at the side walls, but also to a lesser extent at the front and back faces. The upper surface is symmetrically domed as a result of the granular up-thrust in the mid-plane region. The form of this configuration is illustrated schematically in Fig. 2(i), the arrows showing the convection averaged over the direction normal to the front face.

At lower frequencies, within the region B of Fig. 1, the two rolls exhibit asymmetry, one extending over a larger volume of the bed than the other. The configuration found in region B close to the boundary with A is shown schemati-

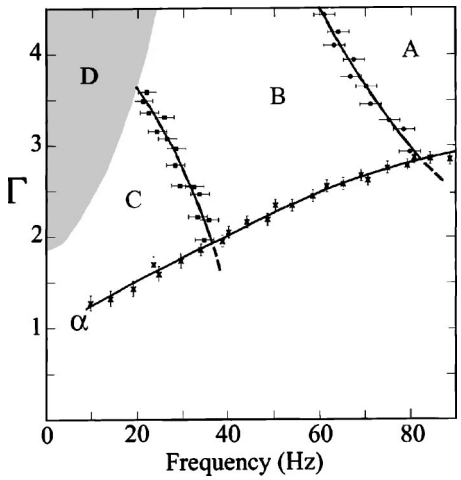

FIG. 1. Schematic diagram showing the regions of the f-Γ plane for symmetric convection rolls (A), asymmetric convection rolls (B), and full Faraday tilting (C), for a water-immersed bed of 600–710-μm bronze spheres of 10 mm mean depth. The line indicated as α shows the onset of appreciable granular convection on the time scale of 1 min. In the region D violent throwing of the upper surface disrupts these simple convective motions.

cally in Fig. 2(ii). We observe that the bed breaks symmetry in either direction, confirming the accurate alignment of our apparatus. Within region B the upper granular surface consists principally of a major and a minor plane both at about the same dynamic angle of repose to the horizontal, typically 15°–18°. There is some rounding close to the side walls and as the planes meet. In all cases, the convection speed of the larger roll is higher than that of the smaller roll.

At yet lower frequencies, the smaller convection roll shrinks further with respect to the larger and the minor plane retreats [Fig. 2(iii)] until, within region C, one loop completely dominates and the granular bed adopts the simple Faraday tilt configuration shown schematically in Fig. 2(iv). The angle of tilt depends somewhat on frequency and Γ but is $\sim 21°$ at 20 Hz and $\Gamma = 2$. Figure 1 also shows, at low

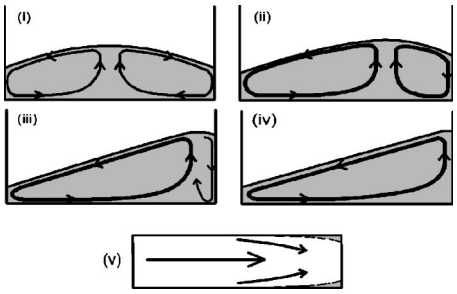

FIG. 2. The configuration and convection flows found in various regions of the f-Γ plane of Fig. 1. The configuration and convection flow in region A is shown in (i). That in B close to the boundary with A is shown in (ii). That in B close to the boundary with C is shown in (iii), while the configuration found in C is shown in (iv). (v) shows a horizontal section of (iii) or (iv) indicating the regions where surface movement is impeded by the box edges. The smaller arrows show the main granular flow being diverted away from the principal box faces.

frequencies and for substantial Γ, a region D where violent throwing of the granular bed disrupts the simple convective behaviors found at lower values of Γ.

Within region A, the convection shows appreciable deviation from two-dimensional behavior, with significant downward granular flows at the principal box faces. As the frequency is lowered and the horizontal extent of the larger convection roll extends beyond half the box width, the convection becomes increasingly two dimensional. The granular down-flow at the principal box faces greatly reduces. In the region of full Faraday tilt, C, and in the nearby parts of B for which one convection roll extends across most of the box, the only deviations from two-dimensional flow are associated with the box edges under the tilt apex which impede granular movement. The granular flow in this region of the f-Γ plane has been studied in detail using a tracer grain, noting where the grain enters the bulk at the bottom of the slope, where it re-emerges close to the top of the slope and the times between these two events. Figure 2(v) shows schematically a horizontal cross section deep in the bed. The shaded areas represent regions within the bed where we find that the grains move more slowly than in the main convective flow, which is diverted away from the front and back box faces in these regions. The overall flow is close to two dimensional. However, we note that the granular velocities observed at the principal box faces only reflect the velocities in the bulk of the bed for about two-thirds of the box width. Under the apex, the velocities observed at the principal faces of the box are appreciably lower than those within the bulk of the bed.

The boundary between the regions A and B of Fig. 1 has been obtained by identifying appreciable deviations from symmetry between the two convective rolls using a digital camera and a large visual display. The boundary between regions B and C has been defined as follows. As the frequency is decreased through region B, so that the boundary with region C is approached, an increasing fraction of the upper slope consists of a single tilted plane, with rounding to a lower angle at the top of the slope [Fig. 2(iii)]. We identify the region C as exhibiting a single plane with rounding over less than 3–4 grain diameters. The method of determining diagrams such as Fig. 1 was as follows. Initial investigations, observing the behavior at many fixed values of f and Γ, were used to broadly locate the different regions of behavior. The boundaries between the different behaviors were then determined more precisely. The boundaries between A and B and between B and C were determined by varying the frequency at fixed Γ, observing the behavior on a large screen display and judging the boundaries using the criteria given above. Sufficient time was allowed for the system to come to equilibrium following each adjustment of frequency. The horizontal error bars in Fig. 1 represent the uncertainties in our judgement while the points mark the mid-point of this range of uncertainty. The line representing the onset of granular convection was determined by slowly increasing Γ at a number of fixed frequencies. The error bars again represent the uncertainties in our judgement.

From these visually determined boundaries we are able to report how the behavior depends upon grain diameter and bed depth. Faraday tilting has been studied for bronze beds

with mean grain diameters between 250 and 1400 μm. It is found that, as the grain diameter is increased, Faraday tilting may only be observed at progressively lower frequencies. The frequencies at which the boundaries between regions *A* and *B* occur vary approximately inversely with the mean grain diameter. This dependence is also found for the boundaries between regions *B* (partial tilt) and *C* (full tilt). As the grain diameter is reduced the speed at which tilting forms and the speed of the subsequent granular convection progressively reduce. Full and partial tilting behaviors occur at higher frequencies for more shallow beds, the boundary frequencies for a 5-mm bed depth being about double those for a 20-mm depth.

We have repeated these measurements using spherical soda-glass grains of density 2500 kg m^{-3}. For bed depths less than 15 mm and for grain sizes exceeding 400 μm we observe similar behaviors to those reported in Fig. 1, but with boundary frequencies about double those for the same mean size of bronze grains. The boundary frequencies (*A*-*B* and *B*-*C*) for glass vary approximately inversely with grain size as they do for bronze. However, for glass, the dynamics are generally far slower than for bronze. For beds of depth greater than 15 mm and for grain sizes less than 400 μm the granular behavior is very slow indeed and, for sufficiently small grains, the granular motion may cease completely within the bulk of the bed. This is in agreement with the findings of Kozlov, Ivanova, and Evesque who have studied a bed of liquid-immersed fine glass grains subject to vertical vibration. They report the observation of numerous small piles on the upper surface, but no bulk granular motion and no bed tilting [19,20].

IV. COMPUTER SIMULATIONS OF FARADAY TILTING

Over the last few years, there has been a growing interest in simulating the dynamics of fluid-particulate systems [21,22]. These simulations focus on sedimentation and fluidization, and employ a range of models of varying complexity. However, to date, there have been no simulations devoted to the study of Faraday piling in which the fluid motion is coupled to both the granular motion and the motion of the vibrating container [13,23].

Our simplified model of the fluid-particulate system uses a three-dimensional (3D) molecular dynamical treatment of the particle motion, coupled to a coarse grained hydrodynamical treatment of an incompressible fluid which ignores fluid inertia. These approximations are appropriate for bronze particles in water as water may be treated as incompressible and bronze is approximately nine times more dense than water. However, for the glass-water systems discussed briefly above, the use of a model which ignores fluid inertia would no longer be applicable.

In our simulations, the spherical bronze particles, of material density 8900 kg m^{-3}, have sizes selected from a uniform random distribution of diameters with a spread of ±10% about the mean value of 655 μ*m* in order to avoid crystallization. For computational simplicity we have used a linear spring dash-pot model to effect normal grain-grain, $\vec{F}_{gg}$, and grain-wall, $\vec{F}_{gw}$, interactions. The spring constant is set to 10^3 Nm^{-1} for which the mean particle overlap during a collision is of order 0.1% of the particle diameter. As a result, the dynamics are not appreciably changed by increasing the magnitude of the spring constant towards the considerably higher values corresponding to the true material parameters. The choice of this soft spring allows larger update time steps [24]; in our simulations we have used $\Delta t = 5 \times 10^{-6}$ s. In this class of problem, we have found that a simple spring dash-pot model gives very similar results to nonlinear collisional models such as Hertzian contacts [25]. We have therefore retained the former due to its computational simplicity.

It has been shown that, for Stokes' numbers less than 10, the effective coefficient of restitution for granular collisions in a liquid such as water is very close to zero [26]. Since experimentally, the majority of our collisions fall in this regime, we adjust the dash-pot parameter of our model so that the collisions are close to being critically damped. A range of restitution coefficients was also tested and the effect on the resulting Faraday piling was minimal, indicating the importance of the fluid-particle coupling and the weak dependence on collisional details.

Sliding friction is treated through a simple Coulomb model, the tangential frictional force $\vec{F}_f$ being proportional to the total normal collisional force. Such a friction model does not possess a static limit. However, if a slope is set up as the initial condition, its relaxation time in the absence of vibration is many orders of magnitude greater than the vibratory time periods in which we are interested. In a more detailed but computationally far slower model, friction, particle rotation, and fluid lubrication would all play a role in determining the dynamic angle of repose of the vibrated particles. In the present simplified model the grain-grain, grain-wall, and grain-base friction coefficients, μ_{gg}, μ_{gw}, and μ_{gb}, are regarded as adjustable parameters which enable us to vary the upper slope angle. Without grain-grain friction no Faraday piling is observed in our simulations, and as μ_{gg} is increased piling strengthens up to a certain point before diminishing. Friction is needed to maintain a dynamic slope, but with too much friction the particles are unable to move past each other freely enough for a tilt to develop. In general, friction between the grains and the glass sides of the container should be given a lower value to model bronze-glass collisions. In conjunction with grain-grain friction, friction with the base is required for Faraday tilting, whereas friction with the side walls has much less of an effect. In the majority of our simulations we do not therefore include grain-wall friction with the side walls, i.e., we set $\mu_{gw}=0$. Consequently, any convective motion of the grains is a fluid-driven phenomenon.

As has already been noted, in a rectangular box of appreciable cross-sectional aspect ratio the course-grained granular and fluid motion is predominantly two dimensional at lower frequencies. Consequently, in our simulations, the course-grained fluid motion is solved using finite difference methods on a two-dimensional grid. We consider particles confined in a box of horizontal cross section 40×3 mm. The shorter dimension is significantly smaller than that used in the experimental system. However, due to the two-dimensional nature of the bulk flow, this computational sim-

plification is a reasonable approximation. We have varied the size of this box dimension and observe little change in the behavior.

A key ingredient of the model is the interaction between the grains and the fluid. At each iteration of the simulation, the mean local particle densities and velocities are mapped onto a coarse 2D-hydrodynamic grid using the "cloud in a cell" method, which involves the two-dimensional linear interpolation of the particle densities and velocities to the four nearest grid points [27]. Given this configuration, we solve for the steady state incompressible fluid flow coupled to the instantaneous velocity of the vibrating container. Local conservation of fluid volume implies

$$\vec{\nabla} \cdot [\phi \vec{V} + (1 - \phi)\vec{U}] = 0, \tag{1}$$

where ϕ is the local porosity in the bed, $\vec{U}$ is the local mean granular velocity and $\vec{V}$ is the local mean fluid velocity. Coupling between the granular and fluid motion is introduced through the force-balance equation

$$\eta \nabla^2 \vec{V} = -\vec{\nabla} P - \beta(\vec{V} - \vec{U}), \tag{2}$$

where P is the hydrostatic pressure and the term containing the product of β and $\vec{V} - \vec{U}$ represents the drag coupling between the fluid and the grains [28]. A full Navier-Stokes equation could be used to include fluid inertia and time dependent behavior. However, within the bed, these additional complexities are not expected to change substantially the motion of the grains. Consequently, we report here results from our simple model which both conserves fluid volume and is able to reproduce Faraday tilting. A more detailed discussion of these fluid effects will be presented elsewhere [29].

To solve Eqs. (1) and (2) we require an explicit expression for β valid for both the low porosities found in the bed interior and the high porosities found at the upper surface. It must also span Reynolds' numbers, $R_e = \rho_f d|\vec{V} - \vec{U}|/\eta$, up to the maximum value encountered in the present work, about 30. Here ρ_f is the fluid density. We therefore use an empirical bed relationship similar to that described by Di Felice [30], a form which has been successfully used by a number of other authors [31,32],

$$\beta = 18(1 - \phi)\frac{\eta}{d^2}(1 + 0.21R_e^{0.687})\phi^{-\chi}. \tag{3}$$

The left-hand part of the right-hand side of this equation describes the forces due to the Stokes' drag on the particles in isolation while the right-hand bracket describes the corrections due to nonlinear effects such as turbulence. The $\phi^{-\chi}$ term describes the deviations from single particle drag, deviations which increase as the porosity is reduced [30]. Here

$$\chi = 3.75 - 0.65 \exp\{-[(1.5 - \log_{10} R_e)^2/2]\}. \tag{4}$$

While Eqs. (3) and (4) are computationally complex, they represent a functional form which gives an adequate description for the range of porosities and Reynolds' numbers encountered experimentally. Note that this form of coupling, β, agrees to within 30% with the empirical bed relationship of Ergun [33] for porosities in the range $0.3 < \phi < 0.8$ and Reynolds' number $R_e \lesssim 40$. However, the detailed dynamics of the upper surface are not treated correctly by the Ergun equation, which does not accurately capture high-porosity behavior. It is also known that the drag is somewhat greater for an accelerating bed than for beds in steady-state flow for which the measurements are available [34] but we make no specific correction for this effect, or for the effects of the fluid history [35].

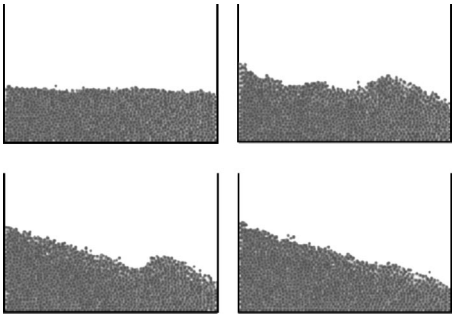

FIG. 3. Granular tilt developing in a 10-mm bed of water immersed 600–710 μm bronze spheres in simulation for $\Gamma = 2.75$ and $f = 25$ Hz. From top left to bottom right, the images are after 0, 3, 10, 15 sec in real time.

Equations (1) and (2) are solved following the method described in Ref. [36]. For a given pressure field and grain configuration, the fluid velocity is relaxed using a finite-difference approximation to Eq. (2). We impose no-slip boundary conditions for the fluid in the frame of reference of the moving box. To enforce continuity, the residual implied by Eq. (1) is used to relax the pressure. This procedure is repeated until the continuity equation is satisfied. We note that taking the divergence of Eq. (2) and substituting in Eq. (1) gives an elliptic equation in the pressure. However, solving such an equation directly does not necessarily enforce continuity [36].

Once the pressure field has been determined, the fluid drag force on each grain is calculated by averaging the pressure gradient within each cell over the grains inside that cell [22]. The resulting equation of motion for grain i is

$$m_i \frac{d\vec{u}_i}{dt} = \vec{F}_{gg} + \vec{F}_{gw} + \vec{F}_f - \frac{\vec{\nabla} P}{n} - m_i \vec{g}, \tag{5}$$

where m_i is the mass of the grain, u_i is the grain's velocity, n is the local granular number density, and $\vec{g}$ is the acceleration due to gravity. Note that we have ignored all buoyancy forces on the grains, an approximation that is valid for high density materials such as bronze.

Figure 3 presents a sequence of snapshots showing the formation of a Faraday tilt starting from a horizontal bed configuration. The coefficients of friction were tuned to give a mean tilt angle of 20°, the values being $\mu_{gg} = 0.3$ and $\mu_{gb} = 0.2$ with the base; there is no grain-wall friction with either the principal box faces or the side walls, as stated above. The simulated behavior is then close to that observed experimentally for the same particle sizes and vibratory conditions. A more detailed comparison will be given below.

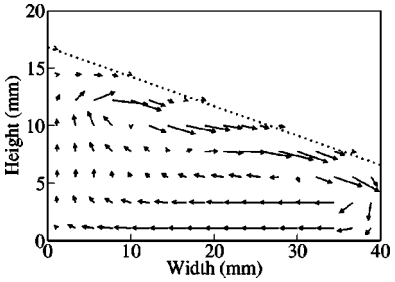

FIG. 4. Results of a computer simulation for $\Gamma = 2.75$ and $f = 25$ Hz using the parameters given in the text. The arrows represent granular volumetric flow. The dotted line shows the maximum mean vertical extent of the bed.

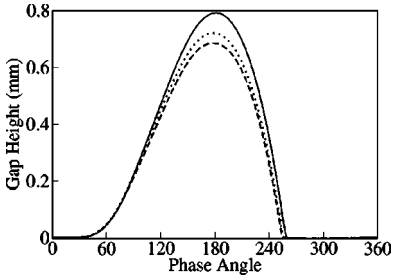

FIG. 5. The flight path of the bottom of an immersed 10-mm bronze bed as a function of phase angle (degrees) through the vibratory cycle for $\Gamma = 2.75$ and $f = 25$ Hz obtained from simulation. A phase angle of zero corresponds to the box passing through its rest position. The full line, dotted line, and broken line are for positions 10 mm, 20 mm (box center), and 30 mm from the deep bed side of the box.

V. GRANULAR CONVECTION IN THE FARADAY TILTED CONFIGURATION

In order to test the validity of our computer model we have compared its predictions for the form and rate of the time-averaged granular flow with the corresponding experimental observations. Our determinations of the mean granular flow involve introducing a tracer particle into the bed and timing it over one complete convection cycle. As the trajectory of the tracer within the bed can only be inferred from the points where it enters and leaves the upper granular surface, we consider trajectories which enter the bed at the very bottom of the slope and emerge at the apex. We can determine the convection time between entry and emergence to about ±10%.

Figure 4 shows the simulated bed configuration and the time averaged convection for $f = 25$ Hz and $\Gamma = 2.75$, which, experimentally, corresponds to the configuration shown in Fig. 2(iv). The agreement with the experimentally observed bed configuration is excellent, the simulated bed being fully tilted. The granular convection is dominated by a single convection roll, with strong motion down the upper slope and down the box end wall with return motion within the bulk. As is observed experimentally a weaker convection roll involving downward motion at the end wall at the deep part of the bed, is essentially absent. The average convection time obtained from the simulation is 14 s. This is in good agreement with our experimental estimate of 16 ± 2 s.

Further investigations show that the simulations exhibit Faraday tilting under conditions of frequency and Γ which agree reasonably well with those shown in the main diagram of Fig. 1. We have also carried out simulations for a range of grain sizes from 500 μm to 1 mm. In each case we find reasonable qualitative and quantitative agreement between our simulations and experiment. These findings give us confidence in our model which has then been used to study the detailed bed dynamics during a single vibratory cycle in the Faraday tilting regime.

We have also carried out additional simulations at higher values of f and Γ where, experimentally, the symmetric convection rolls shown in Fig. 2(i) are observed. The simulations show no fluid-driven convective behavior. However, if some side-wall friction is included, a domed configuration of the upper surface and a pair of Muchowski convection rolls with strong granular up-welling close to the mid-plane of the box is observed. Note that we would not expect the model to be applicable in this high frequency regime where, experimentally, the system exhibits a significant amount of 3D behavior.

VI. DETAILED BED DYNAMICS DURING A VIBRATION CYCLE

In this section we will discuss the grain and fluid dynamics within each vibration cycle, and in particular the processes which lead to the tilting of the granular bed. Initially we will consider the results of simulations for a bed of 600–710-μm bronze spheres, of 10 mm mean depth, vibrated at 25 Hz with $\Gamma = 2.75$. The grain-grain motion is heavily damped by the liquid in which they are immersed. Under these circumstances a distinct gap will form below the bed during flight, since the mean velocity corresponding to the granular temperature is far lower than the downwards velocity of the box. This gap is clear from our simulations. Its magnitude depends upon the local bed depth, being larger for the deeper parts of the tilted thrown bed. This effect has also been observed for thrown tilted beds in air [4].

The predicted motion of the bottom of the bed during flight is shown in Fig. 5 for three positions under the bed and for 25 Hz and $\Gamma = 2.75$, conditions for which the bed substantially settles after each flight, before being thrown again. The bed takes off at a phase angle θ, close to $\theta = \sin^{-1}(1/\Gamma) = 21.3°$, but it may be seen from Fig. 5 that while the shallower parts of the tilted bed are thrown less, all parts land at very similar times. For thrown tilted beds in air, it has been reported that the shallower parts of the bed land substantially earlier, and some authors have based their explanation for tilting on this behavior [4].

As the bed is thrown upwards, the pressure below it falls as liquid is drawn down through the bed. Thus there is an under-pressure below the bed early in flight. Later in flight, when the bed approaches the bottom of the box, liquid is forced upwards through it and there is an excess pressure under the bed. The simulated pressure profile depends appreciably upon the position under the bed. Figure 6 shows, again for 25 Hz and $\Gamma = 2.75$, the time dependence of the

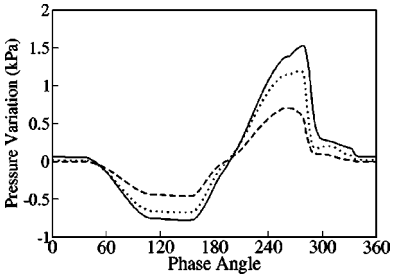

FIG. 6. The pressures changes under the bottom of an immersed 10-mm bronze bed of 600–710 μm grains as a function of phase angle (degrees) for $\Gamma = 2.75$ and $f = 25$ Hz. The full line, dotted line, and broken line are for positions 10 mm, 20 mm (box center), and 30 mm from the deep bed side of the box.

pressure at three positions under the bed as a function of phase angle through the vibration cycle. For an incompressible fluid it is expected that the under-pressure changes to over-pressure at a phase angle close to that corresponding to maximum gap, and it may be seen by comparing Fig. 5 and 6 that this is indeed the case.

If a slightly tilted bed is vibrated vertically, a net horizontal movement of grains produces a more tilted state. In the fully tilted state, however, the net horizontal movement must be zero even though the process which develops the tilt persists. We now consider the detailed balance of processes which maintain the tilted state. We refer to horizontal movement towards the deeper parts of the bed as "construction" and horizontal movement towards the shallower parts of the bed as "destruction." As quantitative measures, we use the particle flux in the horizontal directions corresponding to construction or destruction, respectively. Constructive flux, for example, is obtained by summing the horizontal components of the velocities of those particles moving in a constructive sense. These fluxes are then normalized by dividing by the number of granular layers across the shortest box dimension. The corresponding net tilt construction and tilt destruction movements may be obtained by integrating the constructive and destructive fluxes over one vibratory cycle.

As a tilt develops the constructive flux must exceed the destructive flux, while in equilibrium the two must on average balance. In the simulation of a fully tilted bed, we may examine how these two components vary with time during each vibration cycle. We show, from our simulations, the constructive and destructive fluxes for $f = 25$ Hz and $\Gamma = 2.75$ as a function of phase angle in Fig. 7(a). It is seen that the principal construction begins some time after lift off and increases, passing through a peak and then decreasing towards the time of bed impact. At some values of f and Γ we find a second, smaller, construction peak occurring at times just before and after bed impact. However, its area is quite generally far smaller than the earlier construction peak. Destruction is also shown in Fig. 7(a) as a function of phase angle. It consists of two components, a major part which occurs at, and following, bed impact and a component spread over a wider range of phase angles. Insight into these two components is offered by considering where in the bed these two components occur. Our simulations show that the first component of destruction is spread throughout the bed. As

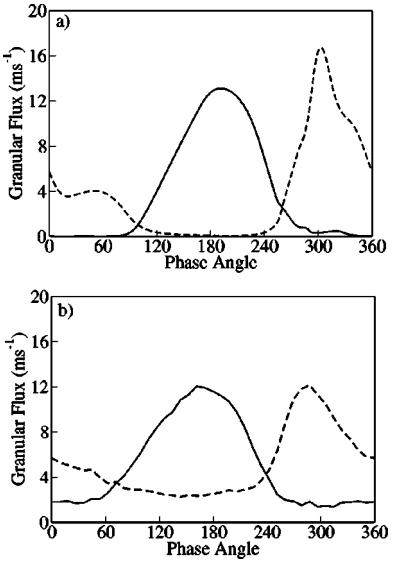

FIG. 7. The construction (continuous line) and destruction (broken line) of the tilt as a function of the phase angle (degrees) obtained from simulation (a) and experiment (b) for $\Gamma = 2.75$ and $f = 25$ Hz.

the bed lands it tends to collapse down slope as a result of the impact. The second component corresponds to motion at and close to the upper surface of the tilted bed, where grains move down the slope. At smaller values of Γ this component of destruction begins at liftoff and continues some time after landing. For higher values of Γ, as here, this surface motion persists well after bed landing and has not completely stopped at the time of the next bed liftoff.

High-speed photography has been used to compare the simulation results with results from the experimentally observed motion. Particle tracking software has been used to determine the velocities of those grains which can be observed through one of the principal box faces, making comparison between frames. The mean horizontal components of the grain velocities have then been used to derive the constructive and destructive fluxes of the granular motion. The results are shown in Fig. 7(b). The observed construction curve shows a broad peak centered on the phase found in the simulations. We cannot clearly resolve any additional construction peak at phases close to the landing angle. This may be due to our resolution which is restricted by the extremely small displacements of each grain between frames. The destruction, shown in Fig. 7(b), shows a strong maximum at and after bed landing, due to motion throughout the bed, and a broader background due to surface motion which takes place over much of the vibration cycle. Since the motion under the tilt apex observed at the front face is slower than in the main body of the granular flow, the data of Fig. 7(b) emphasize processes in the shallower parts of the bed [Fig. 2(v)]. Nevertheless, there is considerable agreement between the simulations and experiment, in the main features, in their magnitude and in their timing.

Additional insight into these behaviors is offered by considering the fluid motion during and after bed flight. Figure 8(a) displays the simulated vector field of the two-dimensional fluid flow for $f = 25$ Hz and $\Gamma = 2.75$ for a phase

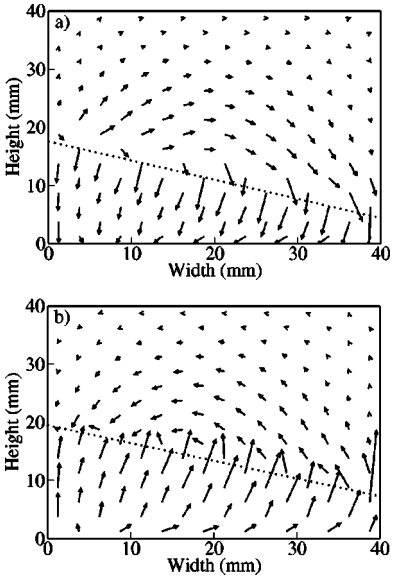

FIG. 8. Vector field of the fluid flow with respect to the box, obtained from simulation for $\Gamma = 2.75$ and $f = 25$ Hz for (a) a phase angle of 120°, and (b) a phase angle of 260°. These two phase angles correspond to the minimum and maximum under-bed pressures, respectively. The dotted lines are a guide to the eye to indicate the approximate position of the upper granular surface.

angle of 120°, close to the time when the under-bed pressure is a minimum. It may be seen that the fluid flow is not just downwards into the bed, but has a considerable horizontal component towards the deeper part of the bed. The net horizontal flow must be zero and this is ensured by fluid flow down the upper slope. Figure 8(b) shows the flow field for a phase angle of 260°, the time of gap closure, when the under-bed pressure is a maximum. Fluid flow passes upwards through the bed as the gap closes, with a horizontal component in the down-slope direction. There is a corresponding return flow above the surface in the up-slope direction. Note that in both Fig. 8(a) and 8(b) the granular motion is not shown, which accounts for the apparent divergence of the flow fields. We have observed these flows experimentally within and above the bed by following mica fragments under high-speed photography.

Early in bed flight, the strong component of fluid motion down the tilted surface affects the motion of the grains thrown from the surface during this phase of the vibration. Surface layers have a lower porosity than the bulk of the bed and are therefore thrown higher, being subject to less fluid damping. Due to the fluid flow, surface grains leave the granular bed at an angle inclined towards the down-slope direction. This leads to "destructive" down-slope surface granular movement, which is aided by saltation. At lower values of Γ the up-slope fluid flow found towards the time of bed landing and seen in Fig. 8(b), assists in bringing the down-slope movement to a halt, while at higher values of Γ the down-slope granular motion persists from one cycle to the next. These effects may all be clearly seen under high-speed photography.

VII. MECHANISM BEHIND FARADAY TILTING

The physical mechanism behind tilt construction is clear from these results. The reduced pressure below the bed early in flight produces fluid flow within the bed which has a horizontal component towards the deeper side of the bed. This may be understood from Fig. 6 which shows that the pressure variations are greater in deeper regions of the bed. This horizontal flow acts on the grains throughout most of the bed causing their acceleration in a constructive sense. Their velocity increases until the point when the under-pressure changes to an over-pressure. At this time, the constructive flux has reached its peak, as may be seen in Fig. 7. Later, as the gap closes, the fluid forces act to reduce the horizontal velocity, and the rate of construction reduces. Just before bed impact, the upward component of the fluid motion may also cause tilt construction, but this is not the principal method of construction. The competing destruction processes consist of bulk processes resulting from the bed impact, and surface processes which may take place over a wide range of phase angles.

As we have noted above, the behavior is predominantly two dimensional when the granular surface is fully tilted in a box of appreciable horizontal aspect ratio. If, initially, a tilt were to develop in both horizontal directions, the influence of the fluid flow would be more important in the direction with the longer slope. Motion in this longer direction would grow at the expense of motion in the shorter direction, leading to the near two-dimensional behavior which is observed.

The mechanism based on tilt construction due to a horizontal component of fluid flow within the bed is consistent with the work of Kumar *et al.* [9] and Behringer *et al.* [13] in that, at lower values of Γ, construction can occur within the bed close to the upper surface. This is in contrast to the mechanism proposed by Faraday [1] in which construction results from grains being drawn under the base of the bed.

We may now consider the parameters under which Faraday tilting occurs in a fluid-grain system. It is clear that the most important feature is the fluid-grain coupling. Examination of Eqs. (1)–(5) shows that a principal measure of this coupling is the dimensionless combination $\gamma = \beta/[\rho_g(1-\phi)\omega]$. Unfortunately β itself depends on the properties and dynamics of both the fluid and the grains through the Reynolds' number, and a complete treatment requires the self-consistent solution of Eqs. (1)–(5). Nevertheless, it may be seen from γ that the damping is increased if the frequency is lowered and if finer and less dense particles are used. If the grain size is increased, Faraday tilting is to be expected at progressively lower frequencies as we have reported.

For weak coupling, $\gamma \ll 1$, no tilting will occur. For sufficient coupling, the fluid-grain interactions cause tilting as we have described. The parameter γ varies through the vibrational cycle, since R_e is a function of $|\vec{V}-\vec{U}|$. However, if we estimate γ when $|\vec{V}-\vec{U}|$ is a maximum, that is when the fluid has most effect on the grains, then, for the system of Fig. 1, $\gamma \approx 1$ on the boundary between *B* and *C*. It is about three times less than this on the boundary between *A* and *B*. This suggests that the parameter γ is useful in providing a rough estimate of the conditions for the onset of Faraday tilting.

Finally, it is known that the body of a thrown bed only exhibits granular convection when the maximum gap below the bed reaches about 0.1–0.2d. This onset of convection occurs at progressively higher values of Γ as the fluid damping increases [37]. For $\gamma \gg 1$, the fluid damping will effectively suppress relative granular motion within the body of the bed and only grains at the surface will be free to move. These grains may exhibit Faraday piling as has been observed for fine glass beds [3,7]. However, the simulation of such an effect falls outside the present study, the computations requiring very large numbers of fine grains and 3D rather than 2D fluid flow.

VIII. DISCUSSION

We have studied the tilting behavior of a vertically vibrated system of grains strongly coupled to a liquid, both through experiments and, through computer simulations. We have observed Faraday tilting over a wide range of grain sizes, for various bed depths and for both bronze and glass. We find close correspondence between many aspects of our experimental observations and our simulations, despite the approximations and simplifications we have used. This gives us confidence that we may use the greater flexibility of the simulation techniques as an aid to understanding the physical mechanisms for tilting.

Faraday tilting is observed over a range of low frequencies and values of Γ whenever the grains are small enough for the liquid-grain interactions to be sufficient, tilting being found over a more restricted range of conditions for larger and more dense particles. Our investigations of tilt construction and destruction clearly show that the tilting is caused by horizontal fluid motion in the bulk of the bed during bed flight. Construction by upward liquid flow at times before and during bed impact is shown to be weak in our simulations and has not been detected in our experiments. At higher frequencies and higher values of Γ the destructive processes are strengthened, weakening tilt.

How do these results relate to the corresponding Faraday tilting of fine granular beds in air? In air, the fluid-grain interactions are weaker for a given grain size and smaller grains must be used to observe tilting. Air is a compressible fluid. Gutman [14] has extended the one-dimensional, constant-porosity bed flight calculations of Kroll [38] to include compressibility and found modifications to gap size and to landing angle. The bed flight is no longer independent of bed depth. Nevertheless, Gutman reports that at low frequencies and for shallow beds the behavioral modifications due to compressibility are relatively small. Since these are the conditions for observing Faraday tilting it is reasonable to expect a common mechanism for tilting in air and water based systems.

In attempting to explain the mechanism behind the Faraday effect some workers have emphasized the role of the variable gap below the bed, and the earlier closure of the gap in the shallower parts of the bed. It has been suggested that the resulting granular compression fronts contribute to tilting [4]. In our own simulations we can see that, in water-immersed systems, all parts of the bed land at much the same time. The spatially dependent timing of gap closure cannot, in water-immersed systems, be an essential feature of the Faraday effect. Another explanation of the air-driven Faraday tilting is based on the upward flow of air as the bed falls to meet the vibrating platform. It was proposed that it is the granular motion resulting from this upward air-flow which causes tilting [5]. While we have been able to detect a weak effect of this type in water-based simulations, we have not been able to resolve the construction resulting from upward liquid flow using high-speed photography. Others have identified horizontal air flow earlier in flight as the cause of tilting in air based systems [2,8]. This is entirely consistent with our own observations on water immersed systems. Horizontal fluid flow early in flight accelerates the grains towards the deeper parts of the bed. The horizontal velocity is a maximum when the under-pressure changes sign. In the later part of flight, horizontal deceleration occurs and by the time of impact bed construction ceases. The principal tilt destruction, rather than construction, results from bed impact.

We have seen how the influence of higher frequencies and higher values of Γ weaken the mechanisms leading to tilt formation. Faraday tilting may therefore only be observed over limited low frequency regions of the f-Γ plane. The use of both fine and light granular materials enables the observation of Faraday tilting over a wider range of frequencies, albeit at the expense of slower dynamics. However, in the case of air-driven tilting, compressibility may then play a more important role in the bed dynamics.

ACKNOWLEDGMENTS

We are grateful to the Engineering and Physical Sciences Research Council for support, to Makin Metal Powders Ltd. and to Potters Ballotini Ltd. for their gifts of powders, and to the workshop staff of the School of Physics and Astronomy for their skills and enthusiasm.

[1] M. Faraday, Philos. Trans. R. Soc. London **52**, 299 (1831).
[2] B. Thomas, Y. A. Liu, R. Chan, and A. M. Squires, Powder Technol. **52**, 77 (1987).
[3] P. Evesque and J. Rajchenbach, Phys. Rev. Lett. **62**, 44 (1989).
[4] C. Laroche, S. Douady, and S. Fauve, J. Phys. (Paris) **50**, 699 (1989).
[5] H. K. Pak, E. van Doorn, and R. P. Behringer, Phys. Rev. Lett. **74**, 4643. (1995).
[6] E. Clement, J. Duran, and J. Rajchenbach, Phys. Rev. Lett. **69**, 1189 (1992).
[7] P. Evesque, J. Phys. (Paris) **51**, 697 (1990).
[8] B. Thomas and A. M. Squires, Phys. Rev. Lett. **81**, 574 (1998).
[9] K. Kumar, E. Falcon, K. M. S. Bajaj, and S. Fauve, Physica A

270, 97 (1999).
[10] B. Thomas, M. O. Mason, and A. M. Squires, Powder Technol. **111**, 34 (2000).
[11] J. Duran, Phys. Rev. Lett. **84**, 5126 (2000).
[12] J. Duran, Phys. Rev. Lett. **87**, 254301 (2001).
[13] R. P. Behringer, E. van Doorn, R. R. Hartley, and H. K. Pak, Granular Matter **4**, 9 (2002).
[14] R. G. Gutman, Trans. Inst. Chem. Eng. **54**, 174 (1976).
[15] N. Burtally, P. J. King, and M. R. Swift, Science **295**, 1877 (2002).
[16] N. Burtally, P. J. King, M. R. Swift, and M. Leaper, Granular Matter **5**, 57 (2003).
[17] Kalliroscope Corporation: www.kalliroscope.com
[18] E. Muchowski, Int. Chem. Eng. **20**, 564 (1980).
[19] V. G. Kozlov, A. A. Ivanova, and P. Evesque, Europhys. Lett. **42**, 413 (1998).
[20] P. Evesque, A. A. Ivanova, and V. G. Kozlov, *Powders and Grains 2001*, edited by Y. Kishino (A. A. Balkema, Lisse, 2001), p. 517.
[21] J. A. M. Kuipers, K. J. van Duin, F. P. H. van Beckum, and W. P. M. van Swaaij, Comput. Chem. Eng. **17**, 839 (1993); B. P. B. Hoomans, J. A. M. Kuipers, W. J. Briels, and W. P. M. Swaaij, Chem. Eng. Sci. **51**, 99 (1996); S. Yuu, T. Umekage, and Y. Johno, Powder Technol. **110**, 158 (2000); S. Yuu, H. Nishikawa, and T. Umekage, *ibid.* **118**, 32 (2001).
[22] S. McNamara, E. G. Flekkøy, and K. J. Måløy, Phys. Rev. E **61**, 4054 (2000).
[23] P. Biswas, P. Sánchez, M. R. Swift, and P. J. King, Phys. Rev. E **68**, 050301(R) (2003).
[24] S. Yuu, T. Abe, T. Saitoh, and T. Umekage, Adv. Powder Technol. **6**, 259 (1995).
[25] L. D. Landau and E. M. Lifshitz, *Theory of Elasticity* (Pergammon Press, Oxford, 1986).
[26] P. Gondret, M. Lance, and L. Petit, Phys. Fluids **14**, 643 (2002).
[27] C. K. Birdsall and D. Fuss, J. Comput. Phys. **3**, 494 (1969).
[28] H. C. Brinkman, Appl. Sci. Res., Sect. A **1**, 27 (1947).
[29] R. J. Milburn, P. Sánchez, P. J. King, and M. R. Swift (unpublished).
[30] R. Di Felice, Int. J. Multiphase Flow **20**, 153 (1994).
[31] B. H. Xu and A. B. Yu, Chem. Eng. Sci. **52**, 2785 (1997).
[32] K. D. Kafui, C. Thornton, and M. J. Adams, Chem. Eng. Sci. **57**, 2395 (2002).
[33] S. Ergun, Chem. Eng. Prog. **48**, 89 (1952).
[34] L. B. Torobin and W. H. Gauvin, Can. J. Chem. Eng.6, 224 (1959).
[35] A. B. Basset, Philos. Trans. R. Soc. London, Ser. A **179**, 43 (1888); C. F. M. Coimbra and R. H. Rangel, AIAA J. **39**, 1673 (2001).
[36] J. C. Strikwerda, SIAM (Soc. Ind. Appl. Math.) J. Numer. Anal. **21**, 447 (1984).
[37] M. C. Leaper *et al.*, Granular Matter (to be published).
[38] W. von Kroll, Forsch. Geb. Ingenieurwes. 50, 2 (1954).